OPEN ACCESS
JOURNAL OF ADVANCED DIELECTRICS
Vol. 15, No. 6 (2025) 2550014 (6 pages)

DOI: 10.1142/S2010135X25500146

High-frequency transparent ultrasound transducer array for photoacoustic imaging application

Zhang Jiaming*, Gao Wen†, Bao Guocui*, Hou Shilin*, Yang Fan*, Gong Xiaojing†, Lin Riqiang†,§, Lam Kwok-Ho‡,¶ and Dai Jiyan*,‖

*Department of Applied Physics,
The Hong Kong Polytechnic University Hong Kong 999077, P. R. China

†Research Center for Biomedical Optics and Molecular Imaging,
Shenzhen Key Laboratory for Molecular Imaging,
Guangdong Provincial Key Laboratory of Biomedical Optical Imaging Technology,
Shenzhen Institute of Advanced Technology,
Chinese Academy of Sciences, Shenzhen 518055, P. R. China

‡Centre for Medical and Industrial Ultrasonics,
James Watt School of Engineering, University of Glasgow, Glasgow G12 8QQ, UK

§rq.lin@siat.ac.cn
¶kwokho.lam@glasgow.ac.uk
‖jiyan.dai@polyu.edu.hk

Received 5 December 2024; Revised 28 March 2025; Accepted 15 April 2025; Published 15 May 2025

Photoacoustic imaging (PAI) technique has been employed as a powerful tool for experimental and clinical applications, however, conventional ultrasound transducers block the light path, leading to bulky and inefficient PAI system designs. Transparent ultrasound transducers (TUT) have been developed, allowing light transmission through transducers and illuminating target directly. Nevertheless, studies on TUT arrays are limited till now. In this work, we propose a novel method for fabrication of 64-element high-frequency TUT array which shows great uniformity on both acoustic and electrical properties. The photoacoustic signal response of the transducer was characterized with expanded laser source which is different from a single element photoacoustic. This work demonstrates the feasibility of high-frequency TUT array fabrication process and its potential for photoacoustic computed tomography (PACT) applications.

Keywords: Lithium niobate single crystal; ultrasound array transducer; transparent ultrasound transducer.

1. Introduction

Photoacoustic imaging (PAI) is a noninvasive biomedical imaging technology which combines advantages of optical imaging with high contrast and ultrasound imaging with deep penetration. Over the past decades, PAI has been widely investigated for oncology.[1] vascular visualization,[2] brain imaging,[3] and so on. PAI signal generation relays on photoacoustic effects. Pulsed laser is usually employed to illuminate imaging target which absorbs the energy of laser and being heated. During the swollen process, photoacoustic signals are generated and acquired by ultrasound transducers. However, conventional ultrasound transducers are always opaque, blocking the light path. To achieve co-axial light illumination and ultrasound detection, PAI systems usually deliver light from opposite side of transducer,[4] or employ complex optical design to deliver from sides of transducers,[5] leading to bulky and inefficient system design. To partially solve this problem, ring-shaped or hollow structured ultrasound transducers have been employed for light passing through.[6,7] However, the central orifice may lead to degraded image quality,[8] while the acoustic properties of transducer may be affected.[9] Although pure-optical detection technology has gained progress recently, it is difficult to develop parallel arrays based on these optical sensors.

Piezoelectric-based transparent ultrasound traducers (TUT) were introduced to allow laser beam passing through directly, working as a part of light delivery system.[10] TUT-based PAI systems possess compact system design and improved signal-to-noise ratio. Single element TUT has been studied for both transparent piezoelectric material.[11,12] and transparent passive materials.[13,14] In aspect of PAI system, ultrasound arrays are more desired compared to single element transducers, due to large field of view (FOV) and high image speed. Recently, a 6.5 MHz TUT linear array was reported based on lithium niobate (LN) single crystal for phantom imaging.[15] Nevertheless, pulse-echo waveform of

‖Corresponding author.

elements showed dual-frequency phenomenon with relatively long pulse duration, which could be led by the sub-dicing fabrication process. The imaging quality was affected due to the irregular waveform. In addition, a 16-element array based on transparent polyvinylidene fluoride (PVDF) was developed with 4.3 MHz frequency. The pitch was larger than 1.5 times wavelength, which may limit the image quality.[16] There is no study of high-frequency TUT arrays with proper geometries, and no reported array could be operated at theoretical frequencies of the piezoelectric material. In this study, a novel fabrication process was investigated to fabricate a high-frequency TUT array with 64 elements, where kerfs were diced after bonding flexible circuits. The acoustic and photoacoustic performances of elements were characterized, where photoacoustic A-line of each element was successfully detected.

2. Methods

To design high-frequency TUT array, the pitch (p) of elements should be in the range as follows:

$$0.5\lambda \le p \le 1.5\lambda, \tag{1}$$

where λ is the wavelength in acoustic transmission media. To avoid shear waves during piezoelectric material vibration, the element width (w) and kerf width (d) should follow the following relation:

$$w \le 0.6t, \tag{2}$$

$$d \le 0.25V_s/f_c, \tag{3}$$

where t is the thickness of piezoelectric elements, V_s is the shear wave velocity of kerf filler and f_c is the center frequency of the transducer.[17] Based on this design principle, the f_c is set as 17 MHz with 190 μm-thick LN single crystal possessing high transparency, high electromechanical coefficient and high receiving sensitivity. Subsequently, pitch and kerf width are determined as 120 and 15 μm, respectively. For elevation size of the TUT array, it is designed as 5 mm following mostly reported arrays.[18] To ensure sensitivity of the TUT, pure epoxy (ERO-TEK 301) was employed for backing layer due to its relatively low acoustic impedance. Also, Parylene C was selected for transparent acoustic matching layer to further enhance acoustic wave transmission efficiency. Design parameters of the TUT array are shown in Table 1.

Table 1. Design parameters of the 64-element high-frequency TUT array.

Center frequency	17 MHz
Element width	0.105 mm
Elevation size	5 mm
Element thickness	0.19 mm
Matching layer thickness (Parylene C)	0.035 mm
Backing layer thickness (Epoxy)	5 mm

The TUT array was fabricated following the procedures: the LN wafer with $7.68 \times 8\,\text{mm}^2$ aperture size was first lapped down and polished to a desired thickness of 190 μm, and transparent electrode indium tin oxide (ITO) was sputter deposited on the top surface of LN. To ensure both high transparency and low sheet resistance ($\sim$40 Ohm/sq), the ITO sputter deposition process was conducted under 1.8 mTorr pressure with 45 Watt DC power. Custom-made flexible circuits with 64 metal wire traces were then adhered along the side of LN, being carefully aligned with the elevation side of LN under optical microscopy and bonded by M-Bond 610 epoxy. After curing at room temperature for 3 days, the exceeded bonding agent was removed carefully by acetone. Degassed transparent low viscosity epoxy was backfilled for both stabilization and backing layer. Curing at room temperature overnight, the backside was then lapped flatly for further processing. Then the whole structure was placed into dicing saw with the other surface of LN up. Due to the transparent nature of the device, the bonded metal wires could be obtained under optical microscopy of dicing saw. Thus, the dicing path could be aligned based on the metal wires. The dicing depth was set as slightly over the thickness of LN to make sure each element could be separated successfully. The diced sample was placed into dry box overnight to dry distilled water in kerfs introduced during dicing process. Then the sample was fixed on glass substrate by double-sided tape with the backing layer up. Degassed epoxy was dropped at the sides for kerf filling based on capillarity. After curing, brass housing was placed around the sample, where a co-axial cable was connected to the housing by silver loaded epoxy. Degassed epoxy was filled again for insulation and stabilization. Finally, transparent and conducting ITO electrode layer was sputter deposited as ground electrode, and subsequently, the Parylene layer was deposited (quarter-wavelength thick) on the front surface of the TUT array for acoustic matching.

Performance of the TUT array transducer including acoustic and electrical properties was characterized. The flexible circuit was connected to a custom-made electrical matching circuit, and electrical impedance of each element was measured with impedance analyzer to obtain at f_c. The design principle follows the basic electrical matching technology [19]. The electrical matching circuit was connected with a flexible circuit to obtain the electrical properties. The characteristic impedance, conductance and attenuation were measured through a network analyzer. The series resistance, series inductance and capacitance were recorded by an impedance analyzer. Then each element was connected to pulse/receiver for measuring pulse-echo response, with 4 μJ energy and 40 dB gain. A digital oscilloscope was employed for single acquisition with 50 Ω damping. Acquired pulse-echo signal was analyzed by fast Fourier transformer (FFT) to obtain frequency spectra.

To evaluate PAI capability, photoacoustic A-line of each element was measured. System setup is shown as Fig. 1,

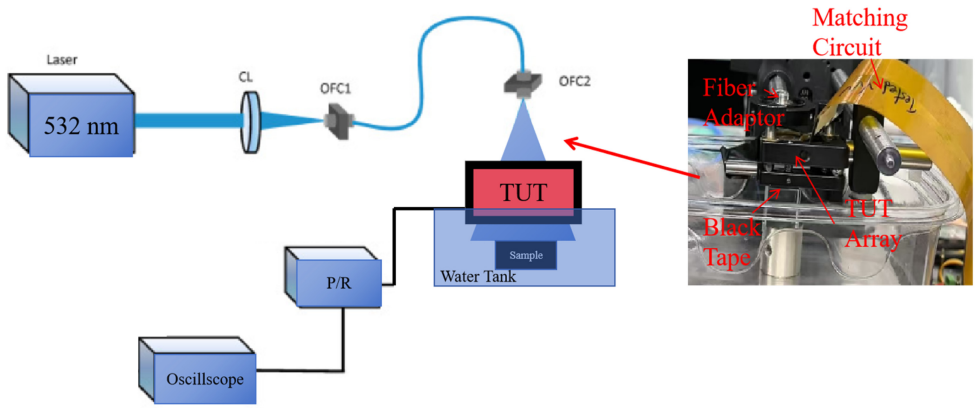

Fig. 1. Schematic of photoacoustic system based on TUT array. CL: Coupled lens; OFC: Optical fiber connector; P/R: Pulser/receiver.

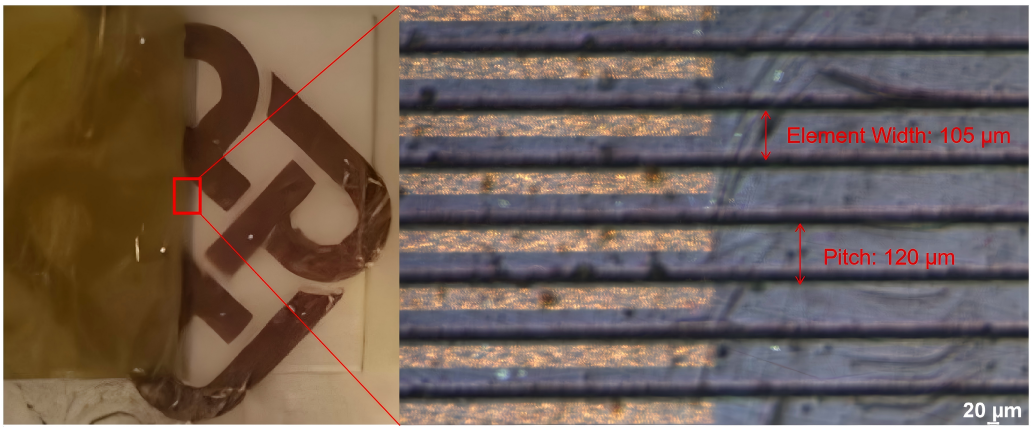

Fig. 2. Photograph of developed TUT array.

where one can see that the laser beam was emitted from the Nd:YAG 532 nm pulsed laser and coupled to an optical fiber with 105 μm core diameter. The fiber was placed above the TUT array which was mounted on a self-designed holder. Laser beam was expanded naturally after transmitting from the fiber distal end. A black tape was placed under the TUT array to generate photoacoustic A-line, which could be acquired by elements of TUT array. The acquired signal was amplified by a pulse/receiver, then displayed on a digital oscilloscope with 128 times averaging. Also, light transmission efficiency was measured by calculating the laser energy before and after transmitting the TUT array.

3. Results and Discussion

Figure 2 shows the photograph of fabricated 64-element TUT array. One can see that, along the elevation, the flexible circuit covers around 2 mm length, while the other part was fully transparent for light path. Due to the transparency of LN single crystal and ITO electrode, the metal traces of flexible circuit at the backside can be clearly seen. The element width was measured as 105 μm and the kerf was measured as 15 μm; these parameters match well with the theoretically designed value. Based on our proposed novel fabrication method, bonding area and piezoelectric elements are clearly separated.

As illustrated in Table 2, the electrical matching circuit and the flexible circuit have been measured. Given the low dielectric value of LN single crystal and the high sheet resistance of ITO electrode, the characteristic impedance was

Table 2. Measured properties for the additional circuits (characterized at 17 MHz).

Characteristic impedance	294.6+227.7i Ω
Conductance	4.5 mS
Attenuation	1.1 dB
Inductance	8.2 μH
Capacitance	9.74 pF
Resistance	25.2 Ω

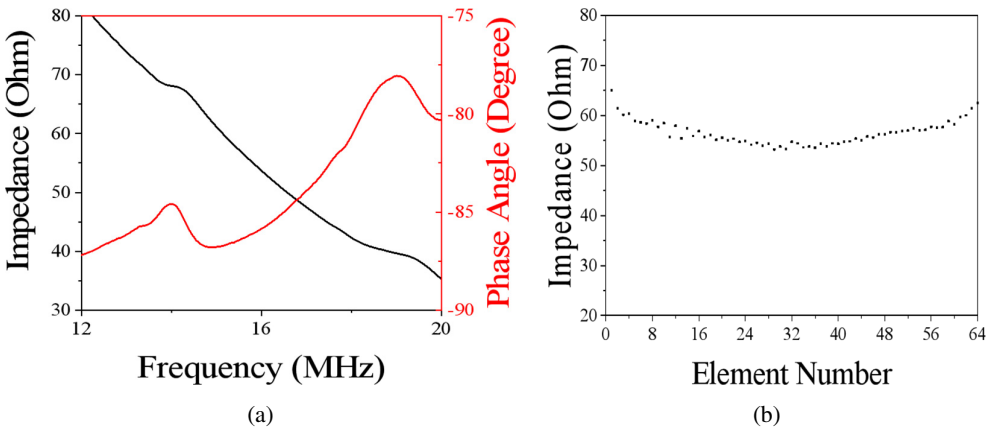

Fig. 3. (a) Measured impedance spectra of element #32 and (b) uniformity of electrical impedance for all elements.

designed to be reasonably high. Impedance spectra and phase angle of one selected element are shown in Fig. 3(a). It is apparent that, since each LN element is operated with small aperture size, the resonance frequency and anti-resonance frequencies are relatively weak. The electrical impedance at f_c is 54.7 Ω, which was near optimal value (50 Ω) due to the custom-made circuit. Total 64 elements show similar electrical impedance at designed f_c, indicating satisfied uniformity of the developed TUT array.

The simulated and measured pulse-echo responses of one element are shown in Figs. 4(a) and 4(b), where f_c is about 17 MHz, and −6 dB bandwidth (BW) is ∼30%. It should be

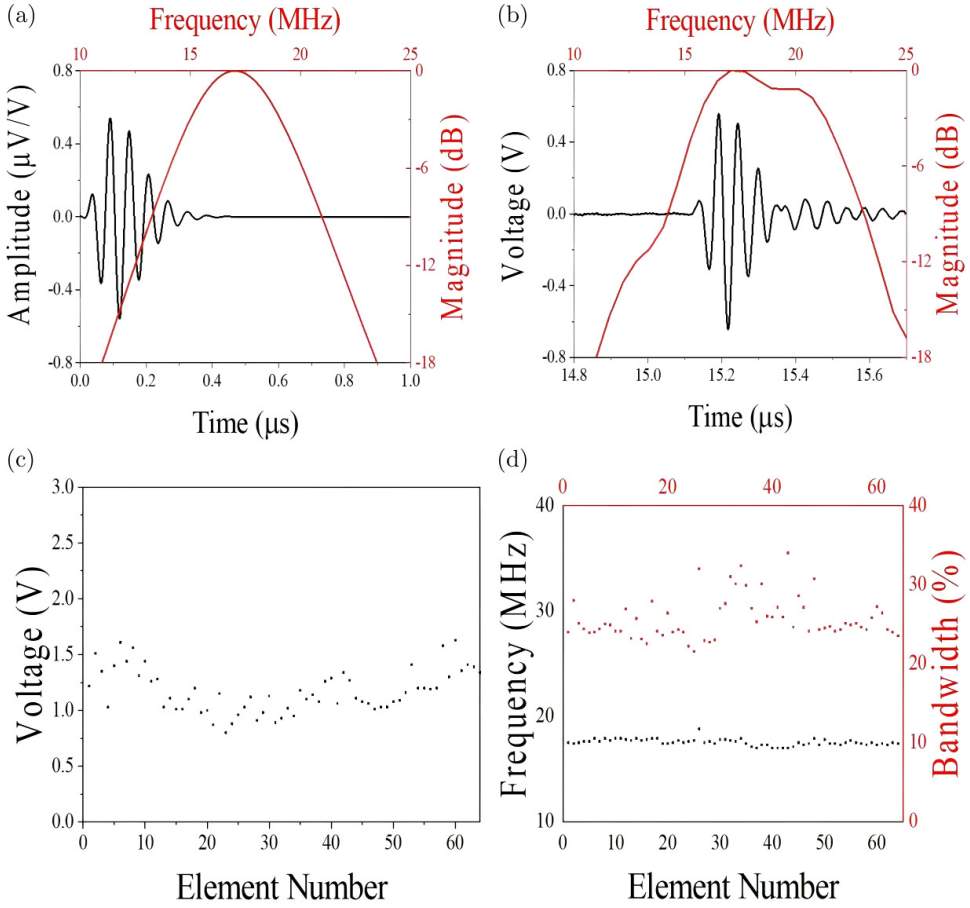

Fig. 4. (a) Simulated and (b) measured pulse-echo response of one element of the TUT array. Uniformity of (c) peak-to-peak and (d) frequency with corresponding frequency spectra.

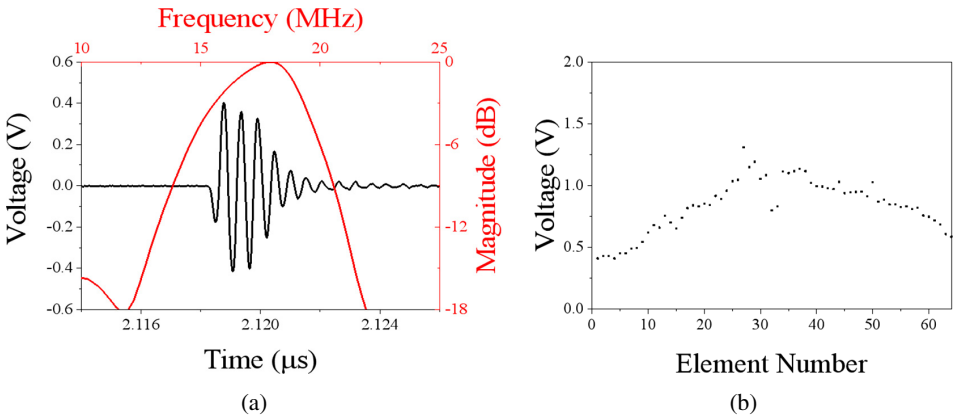

Fig. 5. (a) Photoacoustic A-line of one selected element of TUT array and (b) uniformity of photoacoustic A-line.

noted that, leading by side wall boundary condition, frequency loss always occurred during high-frequency array fabrication. In this study, the measured f_c could match well with theoretical value based on one-dimensional KLM model, which may be contributed by proper stiffness of LN along poling direction. It is apparent that due to the light backing with low acoustic impedance, ring-down of the signal is relatively significant. Nevertheless, the sensitivity of the signal is considered high enough, where over 1 V peak-to-peak amplitude of the pulse-echo signal can be obtained. This suggests that LN is suitable for high-frequency TUT applications.

Uniformity of acoustic properties of the transducer elements was also characterized. Figure 4(c) shows peak-to-peak amplitude of all 64 elements, while Fig. 4(d) shows uniformity of f_c and BW. One can see that each element possesses almost the same f_c, but with slightly different BW and amplitude. This may be attributed to the parylene deposition process, as the acoustic matching layer may be deposited nonuniformly for different elements. The average f_c, BW and peak-to-peak amplitude of the proposed TUT array are 17.5 ± 0.3 MHz, $25\% \pm 2.6\%$ and 1.17 ± 0.2 V, respectively. The uniformity of the TUT array demonstrates comparable uniformity to other developed conventional arrays, and the discrepancy between each element falls within an acceptable error tolerance.[20,21] To evaluate PAI performance, light transmission efficiency was first measured, and it shows $\sim$60% transparency at 532 nm wavelength. During the measurement, the laser energy emitted from fiber was set to about 6.5 mJ/cm^2, which is below the safety limit. Photoacoustic A-line generated by black tape and acquired by an element is shown in Fig. 5(a), where the A-line signal shows center frequency $f_c = 17$ MHz and -6 dB BW = 33%. Noise-equivalent pressure (NEP) of the array element was estimated as 7.6 mPa/Hz$^{1/2}$.[22] The properties of the TUT element possess comparable performance compared to a single element TUT.[23] The high sensitivity was not only contributed by the electrical matching circuit, but also by the great piezoelectric voltage constant of LN single crystal. The sensitivities of all elements were measured as shown in Fig. 5(b). It can be seen that the signal intensities of central elements are much stronger than the elements located at sides. According to Figs. 3(b) and 4(c), elements at sides show similar performance compared to those central elements. Given the validation of the acoustic properties of each TUT array element with satisfactory uniformity, the discrepancy in the PAI signal intensity should be attributed to the nonuniform distribution of light intensity rather than to the characteristics of the elements. The TUT array possesses composite like structure, where light may be scattered differently when propagating through the TUT at different positions. Based on previously reported work, the signal intensity of elements at sides was considered enough for PAI.[13] The practical implementation of photoacoustic computed tomography (PACT) was hindered by limitations in available equipment, precluding further advancement in this study. In comparison to the reported PAI based on TUT array, the developed array in this study is regarded as demonstrating superior performance and higher frequency,[15] which is desired for practical PAI applications. The prospect of practical PACT applications is a subject that needs further exploration in the future.

4. Conclusion

In this study, a 17 MHz TUT array was successfully developed, and all 64 piezoelectric elements were characterized. LN single crystal was employed as active layer due to its high transparency and great piezoelectric voltage constant. The fabrication method provides a novel and universal scheme for further investigation on TUT arrays. Each element shows a regular and uniform waveform at 17 MHz, which matches well with theoretical value. The BW of pulse-echo response and photoacoustic A-line was measured as around 35%. The sensitivities of both ultrasound and photoacoustic response are significantly high; the amplitude of signals achieves over 1 V. These results indicate that the developed TUT array possesses great potential for PACT applications. In the future, the TUT array has the potential for practical application in the context of *in vivo* PAI studies with free-moving small animals.[24] There is still some room for further improvement

in the TUT array. The matching and backing layers could be further studied with more proper acoustic impedance for waveform with short pulse duration. The optical transmission efficiency is relatively limited in this study. The quality of imaging based on the TUT array is contingent upon the laser energy illuminating the imaging target, and the limited transparency results in significant loss of energy transmission from the laser source. This may pose a risk to piezoelectric and polymer passive materials due to the high laser energy at the TUT surface. Despite the fact that the single-crystal LN specimens utilized in this investigation possess high curie temperatures, which serves to safeguard against de-poling, the restricted transparency blocks the feasibility of employing alternative transparent piezoelectric materials for TUT array design. The light transmission efficiency can also be enhanced through optimized ITO sputtering process.[25] Besides, to further improve receiving sensitivity of TUT array, alternating current poled relaxor-ferroelectric single crystal could be implemented for active layer of TUT array.[26]

Acknowledgments

We acknowledge support from the National Key Research and Development Program of China (Grant No. 2023YFC2410900), Hong Kong GRF Grant No. 15220920, the Shenzhen Municipal Science and Technology Innovation Commission (K-ZGMD) and the Shenzhen Municipal Science and Technology Innovation Commission (No. SGDX20230821092359003).

ORCID

Zhang Jiaming https://orcid.org/0000-0001-9297-3659
Yang Fan https://orcid.org/0000-0002-2482-7884
Lam Kwok-Ho https://orcid.org/0000-0003-1456-9049
Dai Jiyan https://orcid.org/0000-0002-7720-8032

References

[1]R. Zhang *et al.*, Exploring the diagnostic value of photoacoustic imaging for breast cancer: The identification of regional photoacoustic signal differences of breast tumors, *Biomed. Opt. Express* **12**, 1407 (2021).
[2]S. Li *et al.*, Photoacoustic imaging of peripheral vessels in extremities by large-scale synthetic matrix array, *J. Biomed. Opt*. **29**, S11519 (2024).
[3]P. Zhang *et al.*, High-resolution deep functional imaging of the whole mouse brain by photoacoustic computed tomography *in vivo*, *J. Biophotonics* **11**, e201700024 (2018).
[4]G. Zhang *et al.*, Developing a photoacoustic whole-breast imaging system based on the synthetic matrix array, *Front. Phys*. **8**, 600589 (2020).
[5]Y. Sun *et al.*, Real-time dual-modal photoacoustic and fluorescence small animal imaging, *Photoacoustics* **36**, 100593 (2024).
[6]J.-M. Yang *et al*., A 2.5-mm diameter probe for photoacoustic and ultrasonic endoscopy, *Opt. Express* **20**, 23944 (2012).
[7]H. Kim *et al.*, Performance comparison of high-speed photoacoustic microscopy: Opto-ultrasound combiner versus ring-shaped ultrasound transducer, *Biomed. Eng. Lett.* **12**, 147 (2022).
[8]S.. Park *et al.*, Optically transparent focused transducers for combined photoacoustic and ultrasound microscopy, *J. Med. Biol. Eng*. **40**, 707 (2020).
[9]R.. Lin *et al.*, Miniature intravascular photoacoustic endoscopy with coaxial excitation and detection, *J. Biophotonics* **16**, e202200269 (2023).
[10]A. Dangi *et al.*, Lithium niobate-based transparent ultrasound transducers for photoacoustic imaging, *Opt. Lett*. **44**, 5326 (2019).
[11]P.. Guo *et al.*, Advancement in PMN-PT transparent piezoelectric ceramic for photoacoustic/ultrasound dual-mode imaging, *J. Materiomics* **11**, 100932 (2024).
[12]W. Gao *et al.*, Achieving coaxial photoacoustic/ultrasound dual-modality imaging by high-performance Sm: 0.72PMN-0.28PT transparent piezoelectric ceramic, *Nano Energy* **132**, 110390 (2024).
[13]J. Zhang *et al.*, Broadband transparent ultrasound transducer with polymethyl methacrylate as matching layer for *in vivo photoacoustic microscopy*, *Photoacoustics* **33**, 100548 (2023).
[14]S.. Cho *et al.*, An ultrasensitive and broadband transparent ultrasound transducer for ultrasound and photoacoustic imaging *in-vivo*, *Nat. Commun*. **15**, 1444 (2024).
[15]H.. Chen *et al.*, A transparent ultrasound array for real-time optical, ultrasound, and photoacoustic imaging, *BME Front.* **2022**, 9871098 (2022).
[16]H. Hu *et al.*, An Optically-transparent PVDF Transducer Array for Photoacoustic Tomography, *SPIE BiOS*, Vol.11960. (SPIE, San Francisco, California, United States: 2022).
[17]T. A. Ritter *et al.*, A 30-MHz piezo-composite ultrasound array for medical imaging applications, *IEEE Trans. Ultrason. Ferroelectr. Freq. Control* **49**, 217 (2002).
[18]C. M. Wong *et al.*, *20-MHz phased array ultrasound transducer for in vivo ultrasound imaging of small animals, Ultrasonics* **126**, 106821 (2022).
[19]J. M. Cannata *et al.*, Design of efficient, broadband single-element (20–80 MHz) ultrasonic transducers for medical imaging applications, *IEEE Trans. Ultrason. Ferroelectr. Freq. Control* **50**, 1548 (2003).
[20]W. Chen *et al.*, Design and fabrication of a high-frequency microconvex array transducer for small animals imaging, *IEEE Trans. Ultrason. Ferroelectr. Freq. Control* **69**, 1943 (2022).
[21]W.. Chen *et al.*, Development of a high-frequency mini-convex array probe for intraluminal ultrasonic imaging applications, *IEEE Sens. J.* **24**, 17560 (2024).
[22]A. Winkler *et al.*, Noise-equivalent sensitivity of photoacoustics, *J. Biomed. Opt*. **18**, 097003 (2013).
[23]S. Mirg *et al.*, Noise Considerations in Piezoelectric Transparent Ultrasound Transducers for Photoacoustic Imaging Applications, *SPIE BiOS*, Vol. 11960 (SPIE, San Francisco, California, United States, 2022).
[24]Y. Wang *et al.*, Cable-free brain imaging for multiple free-moving animals with miniature wireless microscopes, *J. Biomed. Opt.* **28**, 026503 (2023).
[25]M. Althumayri *et al.*, Recent advances in transparent electrodes and their multimodal sensing applications, *Adv. Sci.* **11**, 2405099 (2024).
[26]Y. Sun *et al.*, Recent progress on AC poling of relaxor-$PbTiO_3$ ferroelectric single crystals: A review, *Jpn. J. Appl. Phys*. **61**, SB0802 (2022).